Chemical Geology 530 (2019) 119343

Contents lists available at ScienceDirect

Chemical Geology

journal homepage: www.elsevier.com/locate/chemgeo

Authigenic metastable iron sulfide minerals preserve microbial organic carbon in anoxic environments

Aude Picard[a,1,*], Amy Gartman[a,2], Julie Cosmidis[b,3], Martin Obst[c], Charles Vidoudez[d], David R. Clarke[e], Peter R. Girguis[a]

[a] Department of Organismic and Evolutionary Biology, Harvard University, Cambridge, MA 02138, USA
[b] Department of Geological Sciences, University of Colorado, Boulder, CO 80309, USA
[c] Experimental Biogeochemistry, BayCEER, University of Bayreuth, 95448 Bayreuth, Germany
[d] Harvard Small Molecule Mass Spectrometry Northwest Laboratories, Harvard University, Cambridge, MA 02138, USA
[e] John A. Paulson School of Engineering and Applied Sciences, Harvard University, Cambridge, MA 02138, USA

ARTICLE INFO

Editor: Micheal E. Boettcher

Keywords:
Biomineralization
Iron sulfide minerals
Iron
Sulfur
Organic carbon
Sulfate-reducing microorganisms

ABSTRACT

The burial of organic carbon (OC) in sedimentary environments promotes long-term carbon sequestration, which allows the release of oxygen in the atmosphere. Organo-mineral interactions that form between terrigenous minerals and OC during transport to and deposition on the seabed enhance OC preservation. Here, we propose an authigenic mechanism for the coupled preservation of labile OC and metastable iron sulfide minerals under anoxic conditions. Sulfate-reducing microorganisms (SRM) are ubiquitous in anoxic environments and produce the majority of free sulfide in marine sediments, leading to the formation of iron sulfide minerals *in situ*. Using high spatial resolution microscopy, spectroscopy and spectro-microscopy, we show that iron sulfide biominerals precipitated in the presence of SRM incorporate and adsorb organic molecules, leading to the formation of stable organo-mineral aggregates that could persist for years in anoxic environments. OC/iron sulfide assemblages consist of the metastable iron sulfide mineral phases mackinawite and/or greigite, along with labile organic compounds derived from microbial biomass or from organic molecules released extracellularly by SRM. Together these results underscore the role that a major group of anoxic microbes play in OC preservation and illustrate the value of the resulting authigenic metastable iron sulfide minerals mackinawite and greigite in protecting labile organic molecules from degradation over time.

1. Introduction

The burial of organic carbon (OC) in the sedimentary record over geologic time governs CO_2 levels at the surface of modern Earth (Garrels and Perry, 1974; Berner, 1982; Burdige, 2007). Photosynthetic organisms fix CO_2 at the surface of the ocean to produce OC, which is respired back to CO_2 by heterotrophic microorganisms in the water column. Less than 1% of the OC produced at the surface escapes degradation and reaches the sediment, where it is further subjected to microbial decomposition (Burdige, 2007). Even though active aerobic microbial communities inhabit over a third of the global seafloor (D'Hondt et al., 2015), OC transformations in marine sediments are mainly driven by anaerobic microbial processes (Jørgensen, 1982; Canfield, 1989, 1994). Despite the generally efficient remineralization of OC by microbial processes in sediments, some OC is ultimately preserved and buried over timescales of millenia and longer (Baldock et al., 2004). The greatest sedimentary OC burial occurs along marine continental margins (Berner, 1982; Burdige, 2007; Keil, 2017) and is attributable to high sedimentation rates, to the presence of oxygen minimum zones in the overlying water that minimizes OC degradation during transport, and to the decrease in OC reactivity with increasing depth (Canfield, 1994; Hedges and Keil, 1995; Hartnett et al., 1998; Wakeham and Canuel, 2006; Arndt et al., 2013; Keil, 2017). Moreover, interactions between OC and terrigenous minerals during transport to and deposition on the seabed further lead to the preservation of OC in sediments (Hedges et al., 2001; Keil and Mayer, 2014). Specifically,

* Corresponding author.
E-mail address: audeamelie.picard@unlv.edu (A. Picard).
[1] Present address: School of Life Sciences, University of Nevada Las Vegas, Las Vegas NV 89154, USA
[2] Present address: Pacific Coastal and Marine Science Center, U.S. Geological Survey, Santa Cruz, CA 95060, USA
[3] Present address: Department of Geosciences, The Pennsylvania State University, University Park, PA 16801, USA

https://doi.org/10.1016/j.chemgeo.2019.119343
Received 7 November 2018; Received in revised form 17 October 2019; Accepted 18 October 2019
Available online 19 October 2019
0009-2541/

sorption of OC to mineral surfaces can minimize biological and chemical degradation by slowing down remineralization, stabilizing organic molecules and preserving labile molecules in marine sediments (Hedges and Keil, 1995; Keil and Mayer, 2014). Because OC in sediments is often physically associated with clays and oxy-hydroxides (Ransom et al., 1997, 1999), the flux of minerals to coastal zones is assumed to be the predominant factor determining the amount of organic matter preserved in coastal sediments (Keil et al., 1994).

The role of authigenic mineral formation in the presence of microorganisms (*in situ* biomineralization) in preserving OC has been far less studied. Iron and manganese oxides precipitated during *in situ* biomineralization by Fe(II)-oxidizing and Mn(II)-oxidizing microorganisms, respectively, incorporate and preserve organic molecules in suboxic (< 10 μM O_2) and oxic environments (Chan et al., 2004, 2009; Estes et al., 2017). These metal oxides are stable over time at ambient conditions and are resistant to diagenetic alteration (Krepski et al., 2013; Picard et al., 2015; Estes et al., 2017). The role of *in situ* biomineralization in the preservation of organic carbon in anoxic environments, however, remains unknown. It has been observed that OC and iron sulfide minerals are often buried together in anoxic sediments (Berner, 1982; Berner and Raiswell, 1983), which begs the question as to whether direct organo-mineral interactions can form during authigenic iron sulfide mineral formation and participate in the preservation of OC. Iron sulfide minerals precipitate in anoxic environments where dissolved sulfide produced by sulfate-reducing microorganisms (SRM) interacts with soluble ferrous iron Fe(II) (Rickard, 2012c). Microbial sulfate reduction drives the biogeochemical sulfur cycle in a variety of sedimentary environments (Zopfi et al., 2004; Raven et al., 2016; Riedinger et al., 2017; Wehrmann et al., 2017; Shawar et al., 2018; Jørgensen et al., 2019). The complexities of the sulfur cycle, as well as the challenges of determining the composition of bulk organic matter, have limited our capacity to address critical questions about the relationship between the activity of SRM and the preservation of OC. Sulfide can react with organic matter via sulfurization to facilitate OC preservation (Sinninghe Damste and De Leeuw, 1990; Werne et al., 2004; Amrani, 2014; Raven et al., 2016). In this study, we investigated the potential for iron sulfide biomineralization to be a pathway for OC preservation.

Iron sulfide mineral formation has been extensively studied under abiotic conditions, but the specific role of microorganisms on the formation of iron sulfide minerals under anoxic conditions has only recently been explored (Picard et al., 2016a; Gorlas et al., 2018; Picard et al., 2018; Stanley and Southam, 2018; Mansor et al., 2019; Thiel et al., 2019). Microbial sulfate reduction is more than just the production of sulfide (Schoonen, 2004). Sulfate-reducing bacteria act as templates for the nucleation and growth of mackinawite and greigite, and influence the physical characteristics – particle size and aggregation – of these metastable iron sulfide minerals (Picard et al., 2018). Microbial sulfate reduction accounts for half of the oxidation of organic matter in anoxic marine sediments (Jørgensen, 1982), however, during this process SRM can also generate variable amounts of biomass and/or release organic molecules extracellularly, that can potentially associate with authigenic iron sulfide minerals. The heavy encrustation of SRM by iron sulfides, as reported in environment samples and in laboratory experiments (Ferris et al., 1987; Picard et al., 2016a, 2018), suggests that SRM might play an active role in associating Fe-S minerals and OC. In this study, we used scanning electron microscopy (SEM) with electron dispersive X-ray spectrometry (EDS), and scanning transmission X-ray microscopy (STXM) combining near-edge X-ray absorption fine structure (NEXAFS) spectroscopy with high resolution, and demonstrated that that organic compounds derived from microbial biomass associate with iron sulfide minerals when those were formed in the presence of both live and dead sulfate-reducing bacteria. The association of OC with authigenic, biogenic iron sulfide minerals potentially results in the effective preservation of organic matter in anoxic environments, which has marked, globally relevant implications for the fate of buried OC in past and modern Earth. Ultimately, the physical and chemical characteristics of iron sulfide biominerals could also be indicative parameters of depositional conditions, additionally to geochemical parameters such as sulfur isotopes and trace metal compositions of pyrite (Gregory et al., 2015; Large et al., 2017; Gregory et al., 2019).

2. Material and methods

2.1. Culture medium

Iron sulfide minerals were precipitated in an anoxic marine medium used for the cultivation of sulfate-reducing microorganisms (Widdel and Bak, 1992). The medium composition is given in Suppl. Table A1 (DSMZ medium 195c). The complete experimental procedure describing how to produce strict anoxic conditions was described elsewhere (Picard et al., 2018). A summary of the medium preparation is given here. The *complete medium* was prepared by mixing a mineral solution, a bicarbonate buffer solution, and a sodium-L-lactate solution – each flushed with a N_2/CO_2 gas mixture and autoclaved separately – and sterile vitamin and trace mineral solutions purchased from the American Type Culture Collection (ATTC® MD-VS and MD-TMS). No resazurin nor sulfide were added to the complete medium. To produce the *Fe medium*, soluble Fe(II) was added to the *complete* medium at a final concentration of ~4 mM using a sterile deoxygenated solution of 1 M $FeCl_2$. All procedures were performed in an anaerobic vinyl chamber (Coy Laboratory Products Inc) unless otherwise indicated.

2.2. Iron sulfide mineralization experiments

Biotic experiments were performed by growing the sulfate-reducing bacterium *Desulfovibrio hydrothermalis* AM13^T, purchased from the German culture collection DSMZ (DSM 14728), in the *Fe medium*. Strain AM13 grows optimally at 35 °C and is an incomplete lactate oxidizer (Alazard et al., 2003). Stationary-phase cells of *Desulfovibrio hydrothermalis* AM13 were inoculated at an initial concentration of ~10^6 cells/ml into serum vials containing 50 ml of *Fe medium*. During the experiments, cells grew and reached a concentration of ~10^8 cells/ml. As sulfide was produced during microbial growth, it reacted with Fe(II) to form iron sulfide minerals that produced black and opaque precipitates in the medium. Abiotic experiments were prepared by adding sulfide from a concentrated, sterile Na_2S solution prepared with deoxygenated water to the *Fe medium* to reach concentrations comparable to those produced in biotic experiments (~8 mM). Our previous study has demonstrated that the rate of sulfide addition to abiotic experiments did not impact the characteristics of iron sulfide minerals (Picard et al., 2018). Finally, killed-control experiments were performed using dead cells, either autoclaved or γ-irradiated, that were prepared as follows: serum vials containing stationary-phase cultures grown in 50 ml of complete medium (~10^8 cells/ml) were either placed near a ^{137}Cs gamma-ray source for 48–72 hours, or autoclaved for 20 min at 121 °C. Afterwards, a pellet of dead cells and residues was recovered by centrifugation in 50-ml plastic tubes (~3000 g for 20 min), rinsed and resuspended in 50 ml of *Fe medium*. As dead cells did not produce sulfide, it was added from the concentrated, sterile and anoxic Na_2S solution to reach ~8 mM. In all experiments, the final Fe:S ratio was ~1:2. Solid phases were recovered and prepared for microscopy and spectroscopy as described in the following paragraphs. Table 1 summarizes the experiments and analyses performed in this study.

2.3. Scanning electron microscopy (SEM) and energy dispersive X-ray spectroscopy (SEM-EDS)

EDS in the scanning electron microscope was used to identify the major elements in solid phases formed in biomineralization experiments. Solid phases were harvested by centrifugation (1-ml samples,

Table 1
Iron sulfide minerals characterized in the present study and analytical methods used. The mineralogy of iron sulfide minerals was characterized using X-ray diffraction (Picard et al., 2018).

Experiment	Sulfide source added to Fe medium	Mineralogy of the solid phases	Solid phase analysis
Biotic experiments with live cells	Microbial sulfate reduction	Mackinawite < 5 months Mackinawite + Greigite > 5 months	SEM-EDS STXM
Control experiments with dead cells (γ-irradiated)	Sulfide solution	Mackinawite	SEM-EDS STXM
Control experiments with dead cells (autoclaved)	Sulfide solution	Mackinawite	SEM-EDS STXM
Abiotic experiments	Sulfide solution	Mackinawite	SEM-EDS STXM

~11,000 g for 20 min) and rinsed with sterile deoxygenated pure water in the anaerobic chamber. Minerals were resuspended in sterile deoxygenated ultrapure water, and a drop of suspension was deposited on a small Si wafer fixed to an aluminum stub with double-sided carbon tape. Samples were left to dry overnight in the anaerobic chamber and were transported to the imaging facility in an air-tight jar. Exposure to air was limited to the transfer of samples into the microscopy chamber that was then kept under vacuum for the time of the analyses. As iron sulfide minerals are electron-conductive, imaging was done without sputter coating. Samples were imaged with a Zeiss Supra 55 V P field emission scanning electron microscope at the Harvard Center for Nanoscale Science. Secondary electron (SE) images were obtained at an acceleration of 10 kV using an Everhart-Thornley SE detector or an InLens SE detector. Elemental analysis by EDS was performed at an acceleration voltage of 15 kV using a silicon drift detector (EDAX). Data were generated through the user interface Genesis (EDAX).

2.4. Scanning transmission X-ray microscopy (STXM) and near-edge X-ray absorption fine structure (NEXAFS) spectroscopy

STXM and NEXAFS spectroscopy were used to analyze the distribution of Fe, S, C, O and N and the chemical speciation of Fe, C, O and N in solid phases. Measurements were performed at beamline 11.0.2.2 of the Advanced Light Source (Berkeley, CA, USA) and at beamline 10ID-1 of the Canadian Light Source (Saskatoon, SK, Canada) (Bluhm et al., 2006; Kaznatcheev et al., 2007). Mineral preparation was done in an anaerobic chamber. Minerals were recovered by centrifugation (1-ml samples, ~11,000 g, 20 min), washed and resuspended with sterile deoxygenated ultrapure water. For each sample, a drop of mineral suspension was deposited on a formvar-coated copper 200-mesh TEM grid (Electron Microscopy Sciences) and dried in the anaerobic chamber. TEM grids were fixed beforehand with double-sided tape to an aluminum sample holder adapted to the microscopes at the beamlines. Sample holders were transported to the beamlines in air-tight jars, limiting the contact of minerals with air to less than 30 s during the transfer of sample holders to the microscope chamber. The air in the microscope chamber was evacuated using a vacuum pump and replaced by a He atmosphere (10^{-5} Pa) for measurements. Preliminary measurements had shown that the afore mentioned preparation prevented the oxidation of iron sulfide minerals. Images and/or image sequences (stacks) of mineral aggregates were acquired across the Fe $L_{3,2}$-edges (700–730 eV), the S $L_{3,2}$-edges (150–190 eV, the C K-edge (280–320 eV), the O K-edge (525–560 eV) and the N K-edge (395–420 eV). An energy resolution of 0.1 eV was used for the energy-regions of interest in the absorption spectra. The beamspot size at both beamlines was ~25-30 nm.

Measurements of Fe and S served to determine the distribution of iron sulfide minerals. Measurements of C, N and O allowed characterization of organic material associated with iron sulfide minerals. Measurements at the O K-edge also served to verify that anoxic conditions were maintained during the preparation and the transport of samples to the synchrotrons, as spectral features of iron oxides at the O K-edge are very specific. Spectra of the following reference compounds came from other studies: alginate (as polysaccharide reference), albumin (as protein reference), glucose (as monosaccharide reference) and 1,2-dipalmitoyl-sn-glycero-3-phosphocholine (as saturated lipid standard), vivianite and siderite (references for Fe(II) minerals), goethite and ferrihydrite (references for Fe(III) minerals) (Lawrence et al., 2003; Dynes et al., 2006; Hitchcock et al., 2009; Picard et al., 2016b).

2.5. STXM and NEXAFS data processing and analysis

STXM data were processed using the aXis2000 software package using standard procedures (Hitchcock, 2017). Images were converted from transmission scale to optical density (OD) scale. Species-specific OD maps – Fe(II), total S, organic C in proteins, O in functional groups and organic N in proteins – were generated by subtracting images acquired at energies before the absorption edges (pre-edge images) from images acquired at energies at which bonds of interest are absorbing X-rays (708.7 eV, 176 eV, 288.2 eV, 538 eV, and 401.3 eV, respectively). NEXAFS spectra were extracted from whole image sequences (average spectra) or from specific areas in whole image sequences, when relevant. Spectra recorded across the C K-edge were fitted following the procedure described elsewhere in order to quantify the contribution of peaks associated with individual functional groups to the total spectral area (Estes et al., 2017). Briefly, the procedure is as follows: spectra were normalized to unity and deconvoluted using the software Athena (Ravel and Newville, 2005). An arctangent function was used to fit the ionization threshold. Six Gaussian functions were used to deconvolute spectra in the NEXAFS region, while two additional Gaussian functions were used above 292 eV to approximate σ* transitions. Fit results include only the major functional group resonances. Correlations between the distribution of Fe and C in mineral aggregates were investigated using the ScatterJ plugin (Zeitvogel et al., 2016) available in the free software ImageJ (Rueden et al., 2017) (https://imagej.net/ImageJ). Input images were Fe(II) and organic C (protein) maps of the same area, which represented concentrations of Fe and C, respectively. Maps were aligned to each other and had the same size and resolution. A mask was created to exclude pixels in the background of both images, and pixels that were in thick areas where saturation occurred (e.g. some aggregates might be too thick for C measurements while they are fine for Fe measurements, which leads to false 0 pixels in the C maps). For pixels at the same position in both Fe and C maps, datapoints were extracted and plotted in a scatterplot matrix to visualize the relationship between Fe and C (x = Fe, y = C). A major axis linear regression analysis was performed on the whole dataset using the major axis regression model in the ScatterJ plugin (Zeitvogel et al., 2016). A 95% confidence ellipse was also generated for the whole dataset. There was a large spread of the datapoints, therefore a deviation map of perpendicular distances from the major axis regression line was generated to visualize the areas in iron sulfide mineral aggregates that were enriched or depleted in organic carbon. Regions of similar colors indicate similar deviations of the pixels from the regression line, suggesting compositional variations within the samples (Zeitvogel et al., 2016).

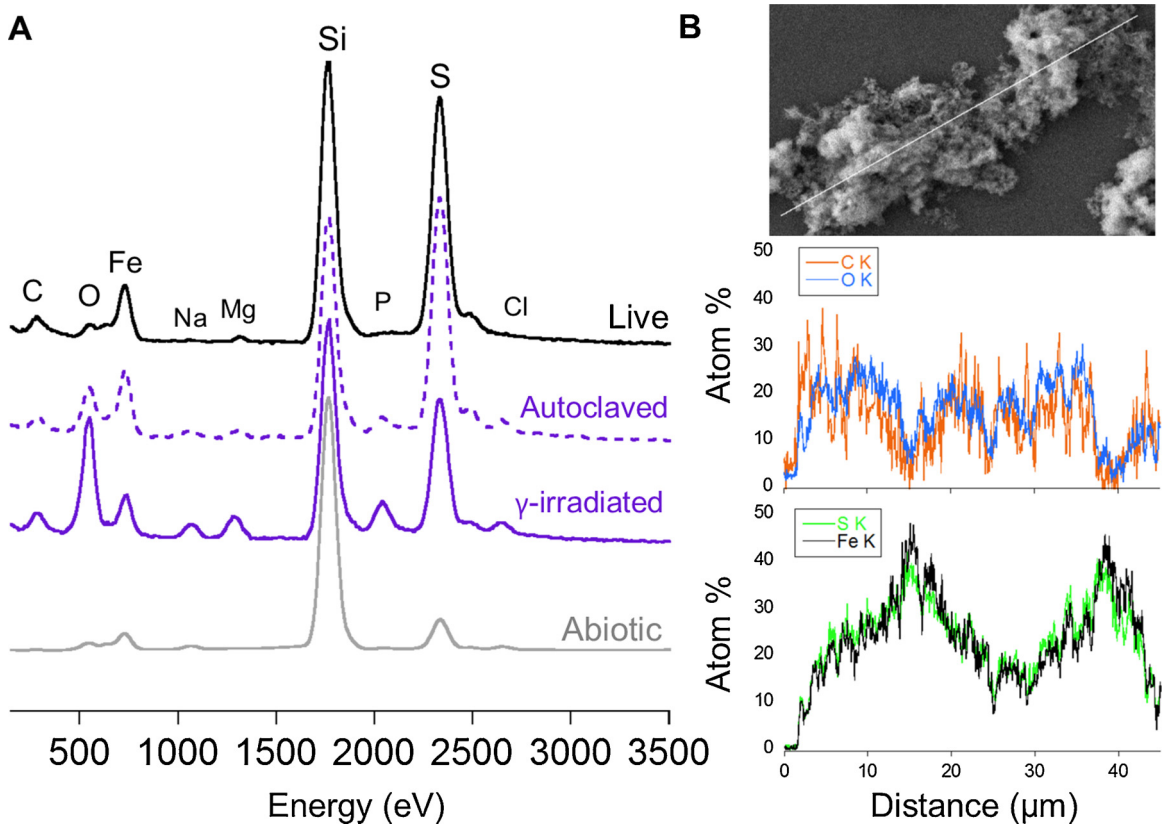

Fig. 1. Elemental composition analysis of aggregate minerals precipitated in the absence (abiotic) and in the presence of live and dead (autoclaved and gamma-irradiated) sulfate-reducing bacteria using energy dispersive X-ray spectroscopy (EDS) in the scanning electron microscope (SEM). (A) Representative EDS spectra show the presence of Fe, S, C and O in minerals precipitated in the presence of live and dead bacteria. C is absent from the mineral aggregates precipitated in abiotic conditions in the culture medium containing lactate. Fe and S are from iron sulfide minerals, Na, Mg, P and Cl from the culture medium. Si from the sample holder. (B) Distribution of elements across a mineral aggregate precipitated with live bacteria. The distribution of O is correlated with C rather than Fe, indicating that O is present in organic functional groups.

2.6. Confocal laser scanning microscopy (CLSM)

Microbe-mineral aggregates were fixed with 4% paraformaldehyde at room temperature for 2 h and labeled with the following fluorescent stains (ThermoFisher Scientific, Invitrogen™): SYBR® Green, FM® 4-64, and Alexa Fluor® 555 conjugate of WGA. These stains bind to nucleic acids, to membranes, and to *N*-acetylneuraminic acid and *N*-acetylglucosaminyl residues, respectively. The WGA conjugate is useful for visualizing bacterial cell wall peptidoglycans. Culture aliquots were stained with all the fluorescent probes mentioned above for 30 min, rinsed and resuspended in PBS buffer. A drop of suspension was mounted on a glass slide and covered with a coverslip. Imaging of microbe-mineral aggregates was performed at the Harvard Center for Biological Imaging. Image stacks of microbe-mineral aggregates were acquired on an inverted Zeiss LSM 880 laser scanning microscope (Carl Zeiss AG, Oberkochen, Germany) with a 100x oil immersion lens, equipped with lasers at 405 nm (reflection), 488 nm (excitation SYBR Green), 561 nm (excitation WGA-555 and FM4-64). Image stacks were processed using ImageJ to extract maximum intensity projections of the Z-stacks.

2.7. Matrix assisted laser desorption ionization – time of flight (MALDI-TOF) mass spectrometry

Minerals were analyzed on a Bruker Ultraflex Extreme MALDI-TOF/TOF at the Harvard Small Molecule Mass Spectrometry facility to tentatively characterize organic components associated with minerals at the level of individual molecules. Biogenic solid phases from two cultures grown in *Fe medium* were compared to abiotic solid phases precipitated in Fe medium and Fe medium + acetate, respectively. Minerals were washed with anoxic Millipore water and dried in the anaerobic chamber. Before the measurements, minerals were re-suspended in Millipore water in the air. A 1-μl drop of matrix (2,5-dihydrobenzoic acid) was first deposited on the sample holder. After it had dried, a 1-μl drop of mineral suspension was deposited on top of the matrix. Samples were measured in positive and negative modes.

2.8. Liquid chromatography (LC) – mass spectrometry (MS)

The liquid phase of microbial cultures was analyzed using LC–MS to characterize unique organic molecules that could be produced in the presence of high concentrations of iron, as well as to identify organic components that could potentially end up associated with minerals. Liquid phases of three individual cultures grown in *Fe medium* for 1, 2 and 4.5 months were compared to the liquid phase of one culture of cells grown in medium without Fe (*complete medium*), to the liquid phase of one experiment with gamma-irradiated cells in *Fe medium* to which sulfide was added, to the *complete medium*, and to the liquid phases of two abiotic experiments performed in Fe medium and in Fe medium + acetate, respectively. The supernatant of those samples was recovered after centrifugation in 2-ml centrifuge tubes (20 min at 11,000 g) and mixed (1:1) with acetonitrile containing an internal standard (d4-succinate) before analysis. Samples were analyzed on a ThermoFisher Ultimate 3000 LC coupled with a Q-Exactive Plus mass spectrometer at the Harvard Small Molecule Mass Spectrometry facility. Five microliters of each sample were injected in a Zic-pHilic column (150 x 2.1 mm, 5-micron particles, EMD Millipore). The mobile phases were 20 mM ammonium carbonate in 0.1% ammonium hydroxide and

acetonitrile 97% in water. The gradient conditions were as follows: 100% B at 0 min., 40% B at 20 min., 0% B at 30 min. for 5 min., then back to 100% over 5 min., followed by 10 min. of re-equilibration. Full ms spectra were acquired in switching polarity at 70,000 resolution, covering a range of mz 66–990. Samples were also analyzed in data-dependent msms top 5 mode. All the data were combined and analyzed in Compound Discoverer 2.0 (ThermoFisher). Likely elemental compositions were computed based on the accurate mass and isotope pattern, and mzCloud msms spectra database, chemspider, metlin and Kegg libraries were searched to identify possible candidates.

3. Results

3.1. Composition of biogenic iron sulfide minerals

Fe, S, C and O were detected in all mineral aggregates precipitated in the presence of live and dead cells of the sulfate-reducing bacterium *Desulfovibrio hydrothermalis* AM13 (Fig. 1A). In comparison, only traces of O and no C were detected in abiotic mineral aggregates precipitated in the culture medium containing lactate (Fig. 1A). The strong Si signal observed in Fig. 1A originated from the Si wafer onto which the minerals were deposited. Fe and S were from mackinawite (FeS) that formed in all conditions, and from greigite (Fe_3S_4) that formed only in the presence of live bacteria after five months of incubation (Table 1,Picard et al., 2018). The likely source for C in biogenic mineral aggregates was microbial biomass, although some could originate from bicarbonate used to buffer the medium. All mineral samples were incubated, handled and transported to the microscope under anoxic conditions, therefore O in iron sulfide minerals was assigned to oxygen-containing functional groups present in organic matter. This is also demonstrated by NEXAFS spectroscopy results, discussed below. A linescan analysis of a mineral aggregate precipitated with live cells confirmed that O spatially correlated with C, and not with Fe (Fig. 1B). The O content was comparatively more important in minerals precipitated with dead cells. Na, Mg, P and Cl were also found associated with most mineral aggregates. Although minerals were washed, a small amount of those elements present in the culture medium remained associated with mineral aggregates.

The distribution of Fe, S and C in biogenic mineral aggregates precipitated with live and dead (γ-irradiated) SRM, after 24 and 16 months respectively, was characterized at high spatial resolution using scanning transmission X-ray microscopy (STXM) (Fig. 2). Fe and S in optical density (OD) maps represent the distribution of iron sulfide minerals (Fig. 2B). C maps display the distribution of organic carbon (C in amide bonds of proteins) in mineral aggregates (Fig. 2B). To identify potential relationships between the distribution of Fe and C, scatterplot plots were generated using Fe(II) and organic C maps (Fig. 2C). Despite the large spread of datapoints, the scatterplots revealed a stronger correlation between Fe and C in minerals precipitated with dead cells than in minerals precipitated with live cells. Deviation maps from a major axis regression line (calculated for each whole dataset, Fig. 2C) were generated to evaluate compositional variations in the samples (Fig. 2D). OC was present all over the aggregates (light blue color in maps), with density increasing at cell-shaped objects (yellow to red colors in maps). The presence of those objects indicates that microbial live and dead cells were well preserved in mineral aggregates (Fig. 2D). Based on OD values, we determined that the amount of organic carbon in mineral aggregates was higher for minerals precipitated with live cells (24-month old minerals: OD average = 0.430 and OD max = 1.81) than for minerals precipitated with gamma-irradiated cells (16-month old minerals: OD average = 0.286 and OD max = 1.41).

3.2. Fe chemistry in iron sulfide minerals – NEXAFS spectroscopy

NEXAFS spectra at the Fe $L_{3,2}$-edges of biogenic minerals recovered after 2, 3 and 9 months of incubation with live cells, after 3.5 months of incubation with autoclaved cells, and after 5 months with γ-irradiated cells, displayed similar spectral features to the NEXAFS spectrum of abiotic mackinawite precipitated in the culture medium that contained lactate (Fig. 3). NEXAFS spectra of all biogenic mineral precipitates did not bear any common features with the spectra of Fe(III) oxyhydroxides goethite and ferrihydrite, nor with the spectra of Fe(II) minerals siderite and vivianite (Fig. 3A). The chemistry of Fe was homogenous in mineral precipitates, as the spectral features of NEXAFS spectra at the Fe $L_{3,2}$-edges did not vary across samples, nor from one spot to another in the same sample.

3.3. Organic carbon analysis in iron sulfide minerals – NEXAFS spectroscopy

The C K-edge NEXAFS spectra of iron sulfide mineral aggregates precipitated in the presence of live and dead bacteria displayed spectral features of organic carbon, with typical peaks for aromatic C and amide bonds (e.g. protein), carboxylic C and O-alkyl C (e.g. poly- and monosaccharides) and alkyl C (e.g. saturated lipid) (Fig. 4 A–B). The spectral signature of biogenic minerals precipitated in the presence of live and dead cells was overall similar, independently of the incubation time (Fig. 4B). Abiotic minerals precipitated in the mineral medium containing lactate only showed a flat, weak and noisy absorption signal with no discernable peaks (not shown). This indicates that either no carbon was associated with abiotic minerals, or that it was below the detection limit. The overall composition of organic carbon in minerals precipitated in the presence of live and dead cells was compared by performing a peak fitting analysis on average C K-edge NEXAFS spectra. Minerals formed in the presence of live and dead cells contained similar abundances of functional groups typical of organic carbon (Fig. 4C). Due to the small number of spectra for samples with dead cells, it was not possible to identify a significant difference between autoclaved and γ-irradiated cells with this analysis. The fitting analysis revealed a small contribution of inorganic carbon (carbonate) to the NEXAFS spectra in all samples. This could be explained by the presence of bicarbonate ions used to buffer the culture medium in these experiments.

The distribution of Fe and C was investigated in mineral aggregates precipitated after short incubations (Fig. 4D). The Fe/C relationships in 3-month old minerals precipitated with live cells and in 5-month old minerals precipitated with γ-irradiated cells were not significantly different from those analyzed after much longer incubations (Figs. 4E vs. 2 C). Minerals precipitated with γ-irradiated cells contained less carbon across the minerals after 5 months than after than 16 months of incubation (Figs. 4G vs. 2 D). STXM maps and image analysis did however reveal significant differences between minerals precipitated dead γ-irradiated cells and autoclaved cells (Fig. 4D-G). First, there was an actual linear trend between Fe and organic carbon in minerals precipitated with autoclaved cells (Fig. 4F, bottom scatterplot). Deviation maps also confirmed this trend; the distribution of organic carbon in minerals precipitated with autoclaved cells was much more homogenous than in other conditions and almost no cells were observed in mineral aggregates (Fig. 4E,G). Using OD values, the max OC content decreased as follows: OD 1.88 in minerals with live cells > OD 1.35 in minerals dead-gamma-irradiated cells > OD 0.55 in in minerals with autoclaved cells, which was consistent with was was observed in older minerals. C K-edge spectra of cell-shaped features and of “extracellular” material in minerals with live cells were quite similar to one another (Fig. 4H). They both displayed high intensity around 288.2 eV, indicating high amide bond concentrations. For minerals precipitated with dead cells, spectral features of C K-edge NEXAFS spectra extracted from cell-shaped features and from extracellular material were different (Fig. 4G). The former contained more protein than the latter, as indicated by the higher intensity of the amide bond peak. The signal of extracellular minerals precipitated in the presence of dead cells was weak and noisy, and the amide peak was absent. This observation is

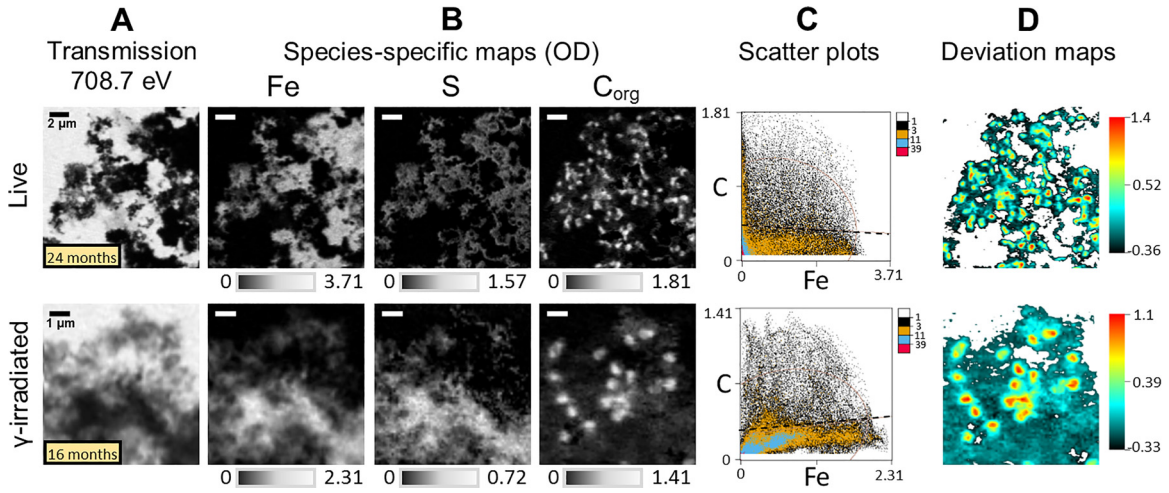

Fig. 2. Scanning transmission X-ray microscopy (STXM) high-resolution imaging of Fe, S, and C in mineral aggregates precipitated in the presence of live and dead (γ-irradiated) sulfate-reducing bacteria. In the upper row, mineral aggregates were analyzed after 24 months of incubation with live cells (scale bar applicable for the full row); in the lower row, minerals were analyzed after 16 months of incubation with γ-irradiated (dead) cells (scale bar applicable for the full row). (A) Transmission images at 708.7 eV, which is the energy at which Fe absorbs the most in samples. (B) Species-specific maps (optical density maps) of Fe(II), total S, and organic C, respectively. The distribution of Fe and S represents the distribution of iron sulfide minerals. Organic C maps represent C in amide bonds of proteins. (C) Scatter plots generated with Fe and C maps to evaluate the distribution correlation between both elements. Major axis regression lines (black dashed lines) and 95% confidence ellipses (light gray) are represented on the scatter plots. (D) Deviation maps showing perpendicular distances of data points from major axis regression lines in the scatterplots.

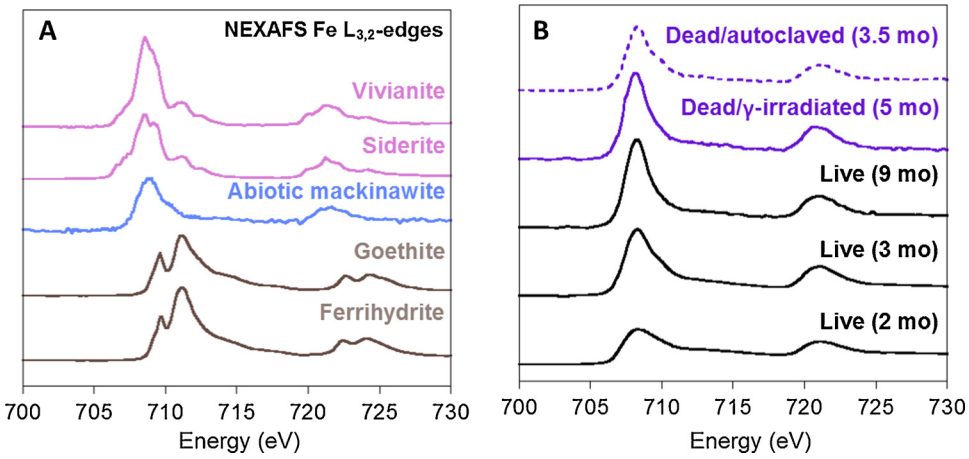

Fig. 3. Near-edge X-ray absorption fine structure (NEXAFS) spectroscopy analysis of Fe in standard Fe minerals and in iron sulfide mineral aggregates. (A) NEXAFS spectra at the Fe $L_{3,2}$-edges of Fe(III) reference compounds (goethite and ferrihydrite), and of Fe(II) reference compounds (abiotic mackinawite from this study, vivianite and siderite). (B) NEXAFS spectra of iron sulfide minerals precipitated with autoclaved cells (3.5 months), gamma-irradiated cells (5 months) and live cells (2, 3 and 9 months).

consistent with the fact that dead cells are not metabolically active and that either they do not release a lot of extracellular molecules in the environment, or that they do release different molecules from live cells.

NEXAFS spectroscopy at the O K-edge was used for a qualitative assessment of the presence of oxygen-containing functional groups, confirming that organic carbon was incorporated in iron sulfide minerals. The spectral feature typical of the carbonyl group found in the peptide bond (protein), in carboxylic C (polysaccharide) and in the ester bond (saturated lipid) occurs at ~532.1 eV (Fig. 5A). Spectral features of O K-edge NEXAFS spectra of Fe(III) oxyhydroxides were absent from the NEXAFS spectra of iron sulfide minerals prepared and measured under anoxic conditions (Fig. 5A). Only a small amount of oxidation would mask the organic features (Picard et al., 2016b). The characteristic peak of organics in the O K-edge spectrum was very weak in the spectrum of minerals precipitated in the presence of autoclaved cells, while it was present in the spectrum of minerals precipitated with γ-irradiated cells and live cells. This is consistent with the general lower abundance of organic carbon in the minerals precipitated with autoclaved cells.

N was present in mineral aggregates precipitated both in the presence of live and γ-irradiated cells (Fig. 6). The N distribution was not measured for autoclaved cells. N displayed a distribution similar to that of C and O; N was concentrated in cell-shaped features and appeared to be diffusely present in mineral aggregates (Fig. 6A). The N K-edge NEXAFS spectrum of mineral aggregates had a characteristic absorption peak at 401.3 eV (Fig. 6B), which is typical of the peptide bond (proteinaceous material). The spectra did not display the broad feature around 406 eV that has been reported in the spectra of fresh bacterial cells as indicative of lipids and potentially DNA (Chan et al., 2011). No other feature was observed in the N K-edge NEXAFS spectra.

3.4. Confocal laser scanning microscopy of mineral aggregates

Confocal laser scanning microscopy was used to evaluate the spatial distribution of some organic molecules (those that can be identified through fluorescent labeling) and of reflecting minerals (Suppl. Fig. A1). The DNA stain labeled the cells poorly. The mineral crusts that formed around cells in our experimental conditions might have prevented the diffusion of the stain inside the cells. The WGA conjugate and the lipid stain highlighted the cells only, suggesting that peptidoglycan-rich and/or lipid-rich molecules did not specifically bind to mineral aggregates. Those molecules, if excreted, could also be too

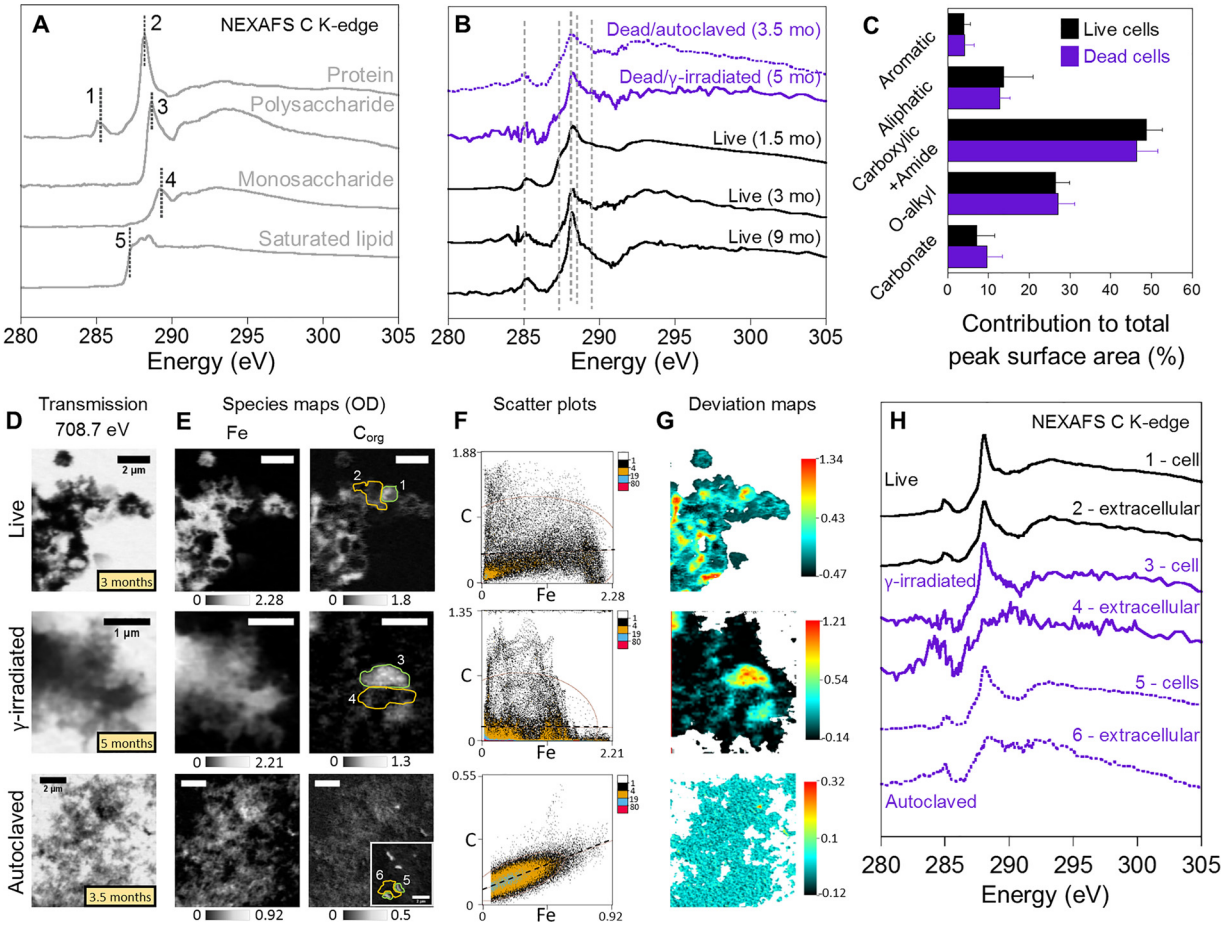

Fig. 4. Near-edge X-ray absorption fine structure (NEXAFS) spectroscopy analysis of organic carbon in mineral aggregates. (A) NEXAFS spectra at the C K-edge representative of major biomolecules: protein (albumin), polysaccharide (alginate), monosaccharide (glucose), and saturated lipid (1,2-dipalmitoyl-sn-glycero-3-phosphocholine). Annotations on the peaks indicate the characteristic spectroscopic features of aromatic C (1), amide bond (2), carboxylic C (3), O-alkyl C (4), and alkyl C (5). (B) NEXAFS spectra at the C K-edge of mineral aggregates precipitated with dead (autoclaved and γ-irradiated) bacteria and live bacteria after various times of incubation. Mineral aggregates precipitated in the presence of bacteria display spectral signatures typical of fresh microbial biomass. (C) Average contribution (%) of functional groups to total NEXAFS peak surface area. The fitting procedure of the NEXAFS spectra is described in the Methods section. (D) Transmission images at 708.7 eV of mineral aggregates precipitated with live (upper row), γ-irradiated (middle row) and autoclaved (lower row) cells, after 3, 5 and 3.5 months, rexpectively. (E) Species-specific maps (optical density maps) of Fe(II) and organic C, respectively. (F) Scatter plots generated with Fe and C maps to evaluate the distribution correlation between both elements. Major axis regression lines (black dashed lines) and 95% confidence ellipses (light gray) are represented on the scatter plots. (G) Deviation maps showing perpendicular distances of data points from major axis regression lines in the scatterplots. (H) NEXAFS spectra at the C K-edge extracted from the delineated regions represented in organic carbon maps in panel E. Regions were selected as cell-shaped features (1, 3, 5) or extracellular material (2, 4, 6).

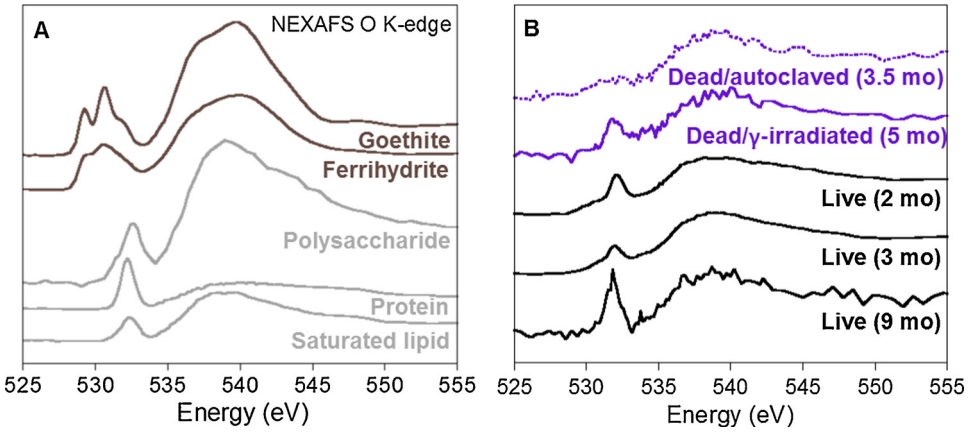

Fig. 5. Near-edge X-ray absorption fine structure (NEXAFS) spectroscopy analysis of O in mineral aggregates. (A) NEXAFS spectra at the O K-edge of Fe(III)-oxyhydroxides – goethite and ferrihydrite – and of major biomolecules – protein (albumin), polysaccharide (alginate), and saturated lipid (1,2-dipalmitoyl-sn-glycero-3-phosphocholine). (B) NEXAFS spectra at the O K-edge of mineral aggregates precipitated with dead (autoclaved and γ-irradiated) bacteria and live bacteria after various times of incubation.

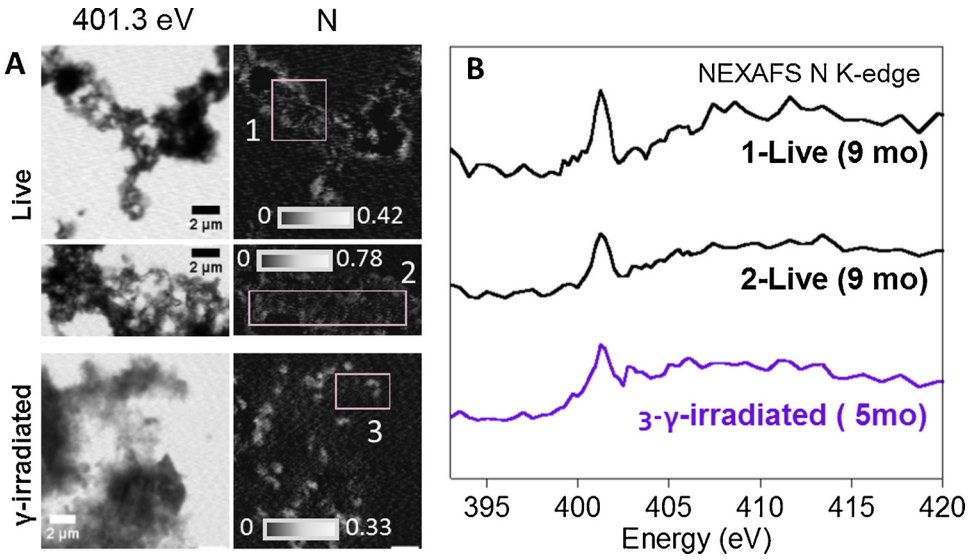

Fig. 6. Near-edge X-ray absorption fine structure (NEXAFS) spectroscopy analysis of organic nitrogen in mineral aggregates. (A) Transmission images at 401 eV, and optical density maps of organic nitrogen in mineral aggregates. (B) Average NEXAFS spectra at the N K-edge extracted from boxes represented on the optical density maps. The main peak at 401 eV seen in all spectra is typical of N in the amide bond in proteins.

dilute to be detected at the surface or inside the iron sulfide minerals. Alternatively, molecules adsorbed to minerals might not necessarily provide the required binding sites for fluorescent labels, or the binding could be sterically hindered.

3.5. Matrix assisted laser desorption ionization – time of flight (MALDI-TOF) mass spectrometry of solid phases

NEXAFS spectroscopy revealed that iron sulfide minerals were associated with organic molecules derived from microbial biomass. However, this method is limited to the identification of functional groups, and by extension to families of organic molecules (monosaccharides, polysaccharides, proteins, lipids). The identification of individual organic molecules associated with solid phases was attempted using MALDI-TOF mass spectrometry, which allows the characterization of large organic molecules with minimal fragmentation. The fingerprint of organic molecules associated with biogenic minerals precipitated with live bacteria was compared to the fingerprint of abiotic minerals precipitated in the culture medium containing lactate. In the positive mode, two peaks of *m/z* 722.5 and 361.9 were identified uniquely in minerals formed in the presence of microorganisms, while in the negative mode, nine peaks unique to the biotic minerals were identified with the following *m/z*: 113.2, 168.8, 233.4, 249.3, 288.2, 310.3, 344.0, 358.0, 381.9. We were not able to match these molecules to any in the databases available to us.

3.6. Metabolomics analysis of extracellular molecules produced by sulfate-reducing bacteria

Liquid chromatography coupled to mass spectrometry (LC–MS) was used to characterize organic molecules released by bacteria in the medium and potentially identify those that could associate with iron sulfide minerals. Cultures grown with or without Fe(II) contained fifty-five molecules at levels significantly higher than: 1) in the complete medium (that contains lactate and vitamins), 2) in abiotic experiments, and 3) in the experiment with gamma-irradiated cells (Suppl. Table A2). Twenty-nine of those fifty-five molecules were identified as involved in metabolic pathways, including biosynthesis of secondary metabolites, microbial metabolism in diverse environments, biosynthesis of amino acids (various pathways), degradation of aromatic compounds, among the most common (Suppl. Table A2). Among all compounds, nine molecules could be identified within the MZcloud database as 4-hydroxyphenylacetic acid and DL-malic acid (aromatic compounds), adenine, guanine and uracil (nucleic acid bases), L-tyrosine and valine (amino acids), nicotinamide (vitamin, synthesis of nucleic acids), methylmalonic acid (Krebs cycle) (Suppl. Fig. A2-A). As the liquid phase of experiments with dead (γ-irradiated) cells had a similar composition to the liquid phase of abiotic experiments, it is possible that γ-irradiated cells remained intact and did not release further intracellular molecules during the formation of minerals, while live cells secreted many compounds in the liquid phase as a result of growth. This is consistent with NEXAFS spectroscopy at the C K-edge (Fig. 5) that shows a low C amount on extracellular minerals of dead bacteria.

It was also possible to identify seven compounds that were produced uniquely in the liquid phase of experiments performed with 4 mM Fe (II), in comparison with the liquid phase of cultures grown without Fe (II) (Suppl. Fig. A2-B). These molecules had monoisotopic masses of 108.05749, 108.0575, 130.06307, 136.96042, 171.95007, 179.01545, 187.9537 (Table S3). Only a few masses could be matched to candidate molecules: cresol or benzyl alcohol, and methyl-oxopentanoate. Candidate formulas could be determined for some masses, but no candidate molecule could be identified (Suppl. Table A3).

4. Discussion

4.1. Preservation of labile OC by metastable iron sulfide minerals in anoxic conditions

Labile organic molecules were incorporated in iron sulfide minerals during their formation in the presence of live SRM and this association persisted for at least two years. Lactate was the only source of OC at the beginning of biotic experiments with live cells. Cell concentration increased from 10^6 cells/ml to 10^8 cells/ml within one week, concomitantly with the production of sulfide and mineral precipitation (Picard et al., 2018). No OC was detected in association with abiotic minerals precipitated in the medium containing lactate (Fig. 1). Therefore, OC bound to iron sulfide minerals in biotic experiments derived from new biomass and/or from organic molecules released extracellularly by various metabolic processes. Potentially, debris of dead cells accumulating later in experiments could also be a source of OC. NEXAFS spectra at the C K-edge of carbonaceous material in minerals were easily deconvolved with standard spectra of proteins, polysaccharides and lipids (Fig. 4C). These compounds represent major constituents of fresh non-encrusted and encrusted bacteria or archaea (e.g. Benzerara et al., 2006; Miot et al., 2009; Cosmidis et al., 2015; Alleon et al., 2016; Miot et al., 2017). Overall, this is also consistent with the composition of organic matter in marine sediments, where

identifiable biomolecules encompass amino acids, carbohydrates and lipids (Burdige, 2007). Spectroscopic features of amide C dominated NEXAFS spectra at the C K-edge, indicating that minerals were principally associated with proteinaceous material (Fig. 4C). All N K-edge NEXAFS spectra displayed a main feature at 401.3 eV that was characteristic of fresh proteinaceous material (Chan et al., 2011; Alleon et al., 2017), even after several months of incubation (Fig. 6). Biogenic iron sulfide minerals therefore represent a potential strong protectant for proteinaceous OC as long as anoxic conditions are preserved in low-temperature surface environments. The dominance of proteinaceous material in Mn oxides was also demonstrated for biogenic and natural samples (Estes et al., 2017). OC associated with iron sulfide minerals precipitated with dead cells also displayed a fresh biomass composition (Fig. 4C). This is consistent with studies of microbial necromass in deep-sea sediments being easily recycled and providing labile organic carbon for the formation of new cells (Lomstein et al., 2012). In the present study, we could not characterize individual molecules in the mineral-associated OC and identify potential signatures that could differentiate minerals precipitated with live cells from those precipitated with dead cells. Our results also indicate that iron sulfide minerals can preserve the integrity of microbial cells (Figs. 2 and 4, Fig. A1). As our experimental conditions favored the precipitation of iron sulfide minerals at the surface of live and dead cells (Picard et al., 2018), iron sulfide minerals may preferentially associate with organic molecules from cell surfaces and/or membranes that help preserve morphology.

The amount of organic carbon associated with minerals, evaluated based on average and maximum OD values extracted from organic C maps (Figs. 2 and 4), decreased in the following order of experimental conditions: live cells > gamma-irradiated cells > autoclaved cells. For live cells, there was no major change in OD values as a function of time (Figs. 2 and 4). Both live and γ-irradiated cells served as templates for mineral precipitation and growth (Picard et al., 2018), and in both cases, organic molecules from the cell surface and membrane could associate with minerals. However, γ-irradiated cells were not metabolically active and therefore could not release extracellular molecules. Those molecules could account for extra OC associated with minerals in the live-cell experiments. The OD values in OC-maps of minerals precipitated with autoclaved cells were significantly lower than OD values of in OC-maps of minerals precipitated with γ-irradiated cells. To prepare dead experiments, cultures grown without Fe(II) and having reached concentrations of 10^8 cells/ml were killed either by placing cultures near a γ-radiation source or by autoclaving cultures. Then, cellular material was recovered by centrifugation and used to inoculate the Fe medium. Although cell concentrations were similar before sterilization procedures, it appears that some cell material was lost during autoclaving and could not be recovered by centrifugation. This suggests that autoclaving does not preserve the integrity of cells as well as γ-sterilization and that only large debris and not intact cells were recovered for the preparation of experiments (Fig. 4E,G). This is a potential important consideration for future experimental design and preparation of killed controls. Additionally, Fe/C relationships differ strongly between experimental conditions. This would require further exploration in experimental and natural samples, but this could represent a potential biosignature for the state of microbial cells at the time of iron sulfide biomineralization.

Interactions between OC and oxidized iron enhance the preservation of OC in sediments. Reactive iron phases, which are defined as the solid phases that can be reductively dissolved by sodium dithionite and which mostly consist of nm-sized goethite, co-precipitate with and/or adsorb OC in marine and freshwater sediments, leading to the formation of Fe-OC macromolecular structures, or Fe-OC chelates (Lalonde et al., 2012). These complexes potentially account for the preservation of more than 20% of the OC buried in surface marine sediments (Lalonde et al., 2012). For a variety of sedimentary oxic to sub-oxic environments, X-ray spectroscopy analyses revealed that a high proportion of reactive Fe, mostly present as Fe(III), is covalently bound to OC, suggesting direct inner-sphere complexation between OC and iron (Barber et al., 2017). Similar interactions occur between dissolved or particulate OC and Fe(III) in hydrothermal vent plumes (Breier et al., 2012; Fitzsimmons et al., 2017; Hoffman et al., 2018). Organic particles can also form complexes with Fe(II) in plumes (Toner et al., 2009). In sediments deposited under anoxic conditions in the Black Sea, OC:Fe ratios are higher than in normal coastal sediments, suggesting the existence of other OC stabilization mechanisms in which Fe is involved (Barber et al., 2017). Here, we propose that incorporation of organic carbon into iron sulfide minerals as shown in our study might explain some of the observations made in those anoxic sediments.

4.2. Binding mechanisms between iron sulfide minerals and organic carbon

Iron sulfide minerals and OC have a strong affinity toward each other and this has lead to the iron-sulfur world hypothesis for the origin of life, which proposed that the exergonic formation of pyrite provided energy for early biochemical reactions at the mineral surface, including polymerization of biological molecules (Wächtershäuser, 1988). Interactions between pyrite and organic molecules have been studied to some extent (Bebié and Schoonen, 2000; Plekan et al., 2007; Mateo-Martí et al., 2008), however there have been a limited number of studies investigating the interactions between mackinawite/greigite and organic molecules (Hatton and Rickard, 2008; Dzade et al., 2013). In our experiments, minerals were washed several times with anoxic water before spectroscopy measurements, indicating that organic compounds are potentially incorporated into the mineral structure or at least strongly bound to minerals. The experimental conditions of this study promoted cellular encrustation of live and gamma-irradiated cells (Picard et al., 2018). The deposition of the first mineral layer was likely favored at the surface of microbial cells, rather than away from cells, through Fe(II) binding onto negative charges available on microbial cells, before sulfide production started (Ferris et al., 1987; Beveridge, 1989). Binding potentially started as soon as cells were inoculated into the medium containing Fe(II). For live cells, binding potentially continued onto new cells while the number of cells increased. When sulfide was released from cells into the experimental medium, nucleation of iron sulfide minerals started at the cell surface. This mechanism of association between iron sulfide minerals and microbial cell surfaces is similar to what has been observed in biogenic Fe(III) and Mn(IV) oxides and in metal binding studies: cation binding to organic functional groups at the surface of microbial cells or extracellular organic structures precedes mineral precipitation (e.g. Ferris et al., 1987; Beveridge, 1989; Chan et al., 2011; Miot et al., 2011; Konhauser and Riding, 2012; Estes et al., 2017). The formation of mineral crusts on gamma-irradiated cells indicates that the surface of dead cells retained a negative charge that allowed Fe(II) binding as well. When sulfide was added to the medium, mineral nucleation could therefore also start at the surface of dead cells or dead cell debris. Cells became completely encrusted in just one week. Therefore, shorter-term studies would be necessary to deepen our knowledge of the early steps of Fe(II) binding and encrustation.

Mineral crusts at the surface of live bacteria represented an estimated 60% of the total iron sulfide minerals precipitated in our experiments after 1 week of incubation (Picard et al., 2018). It was not possible to estimate the proportion of minerals in crusts for the dead cells as these lost their morphology and form smaller structures and vesicles, however transmission electron micrographs revealed significant encrustation for dead cells as well (Picard et al., 2018). The formation of mineral crusts at the surface of cells required accumulation of several layers of mackinawite minerals. The reactive sites on (100) and (010) surfaces of hydrated mackinawite can be described by mono-coordinated (FeS) and tri-coordinated (Fe_3S) sulfur sites (Wolthers et al., 2005). Although the point of zero charge (PZC) of mackinawite is around pH ~ 7.5, the reactive sites can become negatively and positively charged through protonation and deprotonation

processes (Wolthers et al., 2005), even at pH 7.0 at which our experiments were performed. Therefore, Fe(II) and/or mackinawite nanoparticles could directly accumulate onto those sites. Oriented attachment of crystalline nanoparticles has been proposed as crystal growth mechanism of biogenic ZnS in natural biofilms formed by SRM (Moreau et al., 2004). Crystallization by particle attachment has been recognized as crystal growth process in many complex biomineral systems (De Yoreo et al., 2015). This aggregation mechanism would be applicable for both live and dead cells, as new mineral particles nucleated outside of the cells could attach to the first mineral layer formed at the surface of the cells. High-resolution transmission electron microscopy would be an appropriate method to identify mineral growth mechanisms in biogenic iron sulfide minerals.

Alternatively, layers of organic molecules could coat the deposited mackinawite and promote the binding of new mackinawite particles. A single 4-nm nanoparticle of sulfide minerals can potentially associate with 2–5 protein molecules or to > 50 small organic molecules (Chan et al., 2002; Hatton and Rickard, 2008). In biogenic ZnS found in natural SRM-dominated biofilms, aggregation-driven mineral growth may be promoted by extracellular proteins or peptides, rather than microbial cells, suggesting a role of sulfhydryl groups of cysteine residues in binding sulfide mineral surfaces (Moreau et al., 2007). Attractive forces between uncharged surfaces of sulfide mineral nanoparticles and hydrophobic groups in organic molecules have been also proposed as an alternative aggregation mechanism for this system (Moreau et al., 2004). The binding of various organic molecules onto the pyrite surface under anoxic conditions seems to be driven by interactions with thiol groups at the surface of the mineral, and not by the charges of organic molecules or of pyrite (Bebié and Schoonen, 2000). Interestingly, other studies have detected chemisorption of organic molecules on mackinawite and pyrite, through the formation of chemical bonds between N-atoms in amine groups of organic molecules and Fe-atoms in mackinawite and pyrite (Plekan et al., 2007; Mateo-Martí et al., 2008; Dzade et al., 2013). N-atoms in adenine or modified single-strand oligonucleotides interact with Fe-atoms, but not with S-atoms, in pyrite (Plekan et al., 2007; Mateo-Martí et al., 2008). N-atoms in methylamine form strong bonds with Fe-atoms at the (100) and (011) surfaces of mackinawite, while the amine's H forms weak interactions with the surface S-atom of (100) surface of mackinawite (Dzade et al., 2013). Binding of nucleic acids to mackinawite surfaces occurs through nucleobases, and not through phosphate groups nor sugars, confirming the role of N-atoms in binding to iron sulfide minerals (Hatton and Rickard, 2008). A dominance of proteinaceous material on iron sulfide minerals was highlighted in by C K-edge and N K-edge spectroscopy results (Figs. 4 and 6). Further spectroscopic studies would be required to identify the role of S, N and C in binding to biogenic iron sulfide minerals. For example spectroscopy at the S K-edge might provide useful information at the bulk level regarding the proportion of S in the inorganic and organic phases (e.g. Pickering et al., 2001). The binding between Fe and N and/or C will be detectable using extended X-ray absorption fine structure (EXAFS) spectroscopy at the Fe K-edge (e.g. Zhou et al., 2014). Surface interactions and binding energies between organic molecules and iron sulfide minerals could also be studied using X-ray photoemission spectroscopy (Mateo-Martí et al., 2008).

4.3. Stability of organo-mineral interactions

A central question for the long-term preservation of OC is to evaluate if and how long organic-mineral interactions will remain stable. We have demonstrated in this study that such interactions can be stable for about 2 years at ambient conditions. It is however more difficult to predict the fate of mineral-bound OC during burial. Although geological time scales cannot be reproduced in the laboratory, the evolution of iron sulfide minerals could be tested under experimental diagenetic conditions. In recent studies, it was shown that microbial OC associated with minerals can sustain high-grade diagenetic alteration in laboratory experiments for up to several months (Li et al., 2013; Picard et al., 2015; Alleon et al., 2016; Picard et al., 2016b; Miot et al., 2017). It is also unknown if organo-mineral interactions will be stable if metastable iron sulfide minerals evolve to more stable phases, such as pyrite (FeS_2). Mackinawite is metastable under anoxic conditions and over relatively short periods of time (Rickard, 2012b). In our study, biogenic crystalline mackinawite transformed to greigite after > 5 months of incubation at 35 °C, and only in the presence of live cells (Picard et al., 2018). Greigite formation occurs by the solid-state transformation of mackinawite and involves a partial oxidation of Fe(II) to Fe(III) (Lennie et al., 1997; Bourdoiseau et al., 2011), which would potentially promote organic carbon transformations. NEXAFS spectra at the C K-edge mineral-associated OC did not evolve significantly over the transition from mackinawite to greigite (Fig. 4C), suggesting that the solid-state transformation did not alter microbe-mineral associations. Fe $L_{3,2}$-edges NEXAFS spectra of biogenic minerals were similar to the spectrum of abiotic mackinawite precipitated in the culture medium containing lactate (Fig. 3), indicating Fe(II) in a tetrahedral coordination with S (-II) (Todd et al., 2003). The NEXAFS spectrum of biogenic mineral aggregates formed in the presence of live cells after 9 months of incubation, at which time a significant amount of mackinawite had transformed into greigite, had not changed significantly, although greigite contains Fe(III) (Fig. 3). Our spectrum of mixed mackinawite/greigite was also similar to the NEXAFS spectrum of greigite nanoparticles synthesized under hydrothermal conditions (Zhu et al., 2018). A second peak in the 711 eV region, as present in the spectra of Fe(III) oxyhydroxides, would suggest oxidation rather than iron sulfide mineral transformation of mackinawite to greigite (Zhu et al., 2018). EXAFS spectroscopy could be used to track the oxidation state of Fe in the bulk minerals, in addition to characterize bonds between Fe and C/N.

Although conditions were thermodynamically favorable for pyrite to form through the H_2S pathway (Rickard and Luther, 1997), pyrite did not form in any of our experiments, including those in abiotic conditions (Picard et al., 2018). In abiotic studies, pyrite forms rapidly when an oxidizing agent is present (Rickard, 2012d). The source of Fe also plays an important role in the formation of pyrite, since Fe(III) will be first reduced by sulfide, producing Fe(II) and intermediate sulfur species (Peiffer et al., 2015; Wan et al., 2017), while Fe(II) will precipitate directly with sulfide (Rickard, 2012d). In our experiments, conditions were kept strictly anoxic, and Fe was provided as Fe(II), which favors the formation of metastable phases. Further experimental work will be required to understand the fate of organic carbon associated with metastable iron sulfide minerals during pyrite formation. For example, organic molecules are found associated with pyrite in modern biofilms and ancient deposits (Mycke et al., 1988; Braissant et al., 2007; MacLean et al., 2008). In other cases, pyrite is devoid of organic matter, such as these pyrite-encrusted biomorphic objects with size and shape of microorganisms preserved in Middle Miocene to the Pleistocene phosphorite crusts recovered in sediments of the Peruvian shelf (Cosmidis et al., 2013). Pyrite biomorphs were not associated with OC, but they bore resemblance in size and shape with encrusted cells of our study. This illustrates that more experimental work is required to understand how environmental conditions, such as Fe source, Fe:S ratios and microbial presence, control the formation of iron sulfide minerals.

The role of OC in the formation of pyrite has also long been questioned and is still poorly understood (Berner, 1970; Rickard, 2012a). Pyrite formation naturally occurs in anoxic sedimentary environments, where organic matter and a multitude of microorganisms with a range of metabolic potentials are present. This indicates that several microbial and abiotic players are likely to be involved in pyrite formation. The study of microbial community composition and function coupled to high-resolution mineralogy and biogeochemistry in pyrite-forming environments might help identify the potential microbial species involved

in the formation of pyrite, in addition to sulfate-reducing microorganisms. Recently, the involvement of microbial redox activity in the formation of pyrite was demonstrated with enrichment cultures containing SRM and methanogens, among other microorganisms. Pyrite formation occurred from FeS and H_2S, with the concomitant formation of hydrogen, which was proposed to fuel microbial methanogenesis (Thiel et al., 2019). More discoveries as such will help understand the role of iron sulfide biomineralization in the global biogeochemical cycles of Fe, S and C.

5. Conclusion

Iron sulfide minerals are central to our understanding of Earth's past and modern biogeochemical cycles. This study demonstrates the *concomitant* precipitation of iron sulfide minerals with OC *under anoxic conditions* and the importance of iron sulfide minerals as reservoir for the preservation of OC in anoxic sediments. Future studies should aim to closer approximate natural conditions, where the biomass produced is much lower than in culture conditions (e.g. a few orders of magnitude in cell concentration). It is possible these conditions might produce less encrusted cells and impact detection of OC associated with minerals, requiring higher-resolution methods than currently available. This step, and an investigation of whether microbial sulfate reduction was as significant on early Earth as it is on modern Earth, could help elucidate the quantitative significance of organic matter preservation by microbially precipitated iron sulfide minerals for the iron, sulfur, carbon, and oxygen cycles.

Declaration of Competing Interest

The authors declare that they have no known competing financial interests or personal relationships that could have appeared to influence the work reported in this paper.

Acknowledgments

We would like to thank the editor and two reviewers for helping to improve the manuscript significantly. This work was performed in part at the Center for Nanoscale Systems (CNS), a member of the National Nanotechnology Coordinated Infrustructure Network (NNCI), which is supported by the National Science Foundation under NSF award no. 1541959. CNS is part of Harvard University. We thank the Harvard Center for Biological Imaging for infrastructure and support. We thank Shao-Liang Zheng for support at the X-ray laboratory of the Department of Chemistry and Chemical Biology, Harvard University. This research used resources of the Advanced Light Source, which is a DOE Office of Science User Facility under contract no. DE-AC02-05CH11231. Research described in this paper was partly performed at the Canadian Light Source, which is supported by the Canada Foundation for Innovation, Natural Sciences and Engineering Research Council of Canada, the University of Saskatchewan, the Government of Saskatchewan, Western Economic Diversification Canada, the National Research Council Canada, and the Canadian Institutes of Health Research. We thank the staff of beamlines and analytical facilities for support. This work was supported by the National Science Foundation under Grant Numbers NSF-1344241, NSF-1542506 and OCE-1635365 awarded to P.R.G. M.O. was supported by DFG grant OB 362/4-1. J.C. was supported by the Colorado Advanced Industries Accelerator Program (POGGI 2016-1054 0842), sponsored by the Colorado Office of Economic Development, and the Rock-Powered Life 1055 NASA Astrobiology Institute (Coorperative Agreement NNS15BB02A). The authors gratefully acknowledge the support of the Deep Carbon Observatory and the Deep Energy Community.

Appendix A. Supplementary data

Supplementary material related to this article can be found, in the online version, at doi:https://doi.org/10.1016/j.chemgeo.2019.119343.

References

Alazard, D., Dukan, S., Urios, A., Verhe, F., Bouabida, N., Morel, F., Thomas, P., Garcia, J.L., Ollivier, B., 2003. *Desulfovibrio hydrothermalis* sp. nov., a novel sulfate-reducing bacterium isolated from hydrothermal vents. Int. J. Syst. Evol. Micr. 53, 173–178. https://doi.org/10.1099/ijs.0.02323-0.

Alleon, J., Bernard, S., Le Guillou, C., Daval, D., Skouri-Panet, F., Kuga, M., Robert, F., 2017. Organic molecular heterogeneities can withstand diagenesis. Sci. Rep. 7, 1508. https://doi.org/10.1038/s41598-017-01612-8.

Alleon, J., Bernard, S., Le Guillou, C., Daval, D., Skouri-Panet, F., Pont, S., Delbes, L., Robert, F., 2016. Early entombment within silica minimizes the molecular degradation of microorganisms during advanced diagenesis. Chem. Geol. 437, 98–108. https://doi.org/10.1016/j.chemgeo.2016.05.034.

Amrani, A., 2014. Organosulfur compounds: molecular and isotopic evolution from biota to oil and gas. Annu. Rev. Earth Pl. Sc. 42, 733–768. https://doi.org/10.1146/annurev-earth-050212-124126.

Arndt, S., Jørgensen, B.B., LaRowe, D.E., Middelburg, J.J., Pancost, R.D., Regnier, P., 2013. Quantifying the degradation of organic matter in marine sediments: a review and synthesis. Earth-Sci. Rev. 123, 53–86. https://doi.org/10.1016/j.earscirev.2013.02.008.

Baldock, J.A., Masiello, C.A., Gélinas, Y., Hedges, J.I., 2004. Cycling and composition of organic matter in terrestrial and marine ecosystems. Mar. Chem. 92, 39–64. https://doi.org/10.1016/j.marchem.2004.06.016.

Barber, A., Brandes, J., Leri, A., Lalonde, K., Balind, K., Wirick, S., Wang, J., Gelinas, Y., 2017. Preservation of organic matter in marine sediments by inner-sphere interactions with reactive iron. Sci. Rep. 7, 366. https://doi.org/10.1038/s41598-017-00494-0.

Bebié, J., Schoonen, M.A.A., 2000. Pyrite surface interaction with selected organic aqueous species under anoxic conditions. Geochem. Trans. 1, 47. https://doi.org/10.1186/1467-4866-1-47.

Benzerara, K., Menguy, N., Lopez-Garcia, P., Yoon, T.H., Kazmierczak, J., Tyliszczak, T., Guyot, F., Brown Jr., G.E., 2006. Nanoscale detection of organic signatures in carbonate microbialites. Proc. Natl. Acad. Sci. U. S. A. 103, 9440–9445. https://doi.org/10.1073/pnas.0603255103.

Berner, R.A., 1970. Sedimentary pyrite formation. Am. J. Sci. 268, 1–23. https://doi.org/10.2475/ajs.268.1.1.

Berner, R.A., 1982. Burial of organic carbon and pyrite sulfur in the modern ocean: its geochemical and environmental significance. Am. J. Sci. 282, 451–473. https://doi.org/10.2475/ajs.282.4.451.

Berner, R.A., Raiswell, R., 1983. Burial of organic carbon and pyrite sulfur in sediments over Phanerozoic time: a new theory. Geochim. Cosmochim. Acta 47, 855–862. https://doi.org/10.1016/0016-7037(83)90151-5.

Beveridge, T.J., 1989. Role of cellular design in metal accumulation and mineralization. Annu. Rev. Microbiol. 43, 147–171. https://doi.org/10.1146/annurev.mi.43.100189.001051.

Bluhm, H., Andersson, K., Araki, T., Benzerara, K., Brown, G.E., Dynes, J.J., Ghosal, S., Gilles, M.K., Hansen, H.C., Hemminger, J.C., Hitchcock, A.P., Ketteler, G., Kilcoyne, A.L.D., Kneedler, E., Lawrence, J.R., Leppard, G.G., Majzlan, J., Mun, B.S., Myneni, S.C.B., Nilsson, A., Ogasawara, H., Ogletree, D.F., Pecher, K., Salmeron, M., Shuh, D.K., Tonner, B., Tyliszczak, T., Warwick, T., Yoon, T.H., 2006. Soft X-ray microscopy and spectroscopy at the molecular environmental science beamline at the Advanced Light Source. J. Electron. Spectrosc. 150, 86–104. https://doi.org/10.1016/j.elspec.2005.07.005.

Bourdoiseau, J.A., Jeannin, M., Remazeilles, C., Sabota, R., Refait, P., 2011. The transformation of mackinawite into greigite studied by Raman spectroscopy. J. Raman Spectrosc. 42, 496–504. https://doi.org/10.1002/jrs.2729.

Braissant, O., Decho, A.W., Dupraz, C., Glunk, C., Przekop, K.M., Visscher, P.T., 2007. Exopolymeric substances of sulfate-reducing bacteria: interactions with calcium at alkaline pH and implication for formation of carbonate minerals. Geobiology 5, 401–411. https://doi.org/10.1111/j.1472-4669.2007.00117.x.

Breier, J.A., Toner, B.M., Fakra, S.C., Marcus, M.A., White, S.N., Thurnherr, A.M., German, C.R., 2012. Sulfur, sulfides, oxides and organic matter aggregated in submarine hydrothermal plumes at 9°50'N East Pacific Rise. Geochim. Cosmochim. Acta 88, 216–236. https://doi.org/10.1016/j.gca.2012.04.003.

Burdige, D.J., 2007. Preservation of organic matter in marine sediments: controls, mechanisms, and an imbalance in sediment organic carbon budgets? Chem. Rev. 107, 467–485. https://doi.org/10.1021/cr050347q.

Canfield, D.E., 1989. Sulfate reduction and oxic respiration in marine sediments: implications for organic carbon preservation in euxinic environments. Deep-Sea Res. 36, 121–138. https://doi.org/10.1016/0198-0149(89)90022-8.

Canfield, D.E., 1994. Factors influencing organic carbon preservation in marine sediments. Chem. Geol. 114, 315–329. https://doi.org/10.1016/0009-2541(94)90061-2.

Chan, C.S., De Stasio, G., Welch, S.A., Girasole, M., Frazer, B.H., Nesterova, M.V., Fakra, S., Banfield, J.F., 2004. Microbial polysaccharides template assembly of nanocrystal fibers. Science 303, 1656–1658. https://doi.org/10.1126/science.1092098.

Chan, C.S., Fakra, S.C., Edwards, D.C., Emerson, D., Banfield, J.F., 2009. Iron oxyhydroxide mineralization on microbial extracellular polysaccharides. Geochim.

Cosmochim. Acta 73, 3807–3818. https://doi.org/10.1016/j.gca.2009.02.036.
Chan, C.S., Fakra, S.C., Emerson, D., Fleming, E.J., Edwards, K.J., 2011. Lithotrophic iron-oxidizing bacteria produce organic stalks to control mineral growth: implications for biosignature formation. ISME J. 5, 717–727. https://doi.org/10.1038/ismej.2010.173.
Chan, W.C.W., Maxwell, D.J., Gao, X., Bailey, R.E., Han, M., Nie, S., 2002. Luminescent quantum dots for multiplexed biological detection and imaging. Curr. Opin. Biotech. 13, 40–46. https://doi.org/10.1016/S0958-1669(02)00282-3.
Cosmidis, J., Benzerara, K., Menguy, N., Arning, E., 2013. Microscopy evidence of bacterial microfossils in phosphorite crusts of the Peruvian shelf: implications for phosphogenesis mechanisms. Chem. Geol. 359, 10–22. https://doi.org/10.1016/j.chemgeo.2013.09.009.
Cosmidis, J., Benzerara, K., Nassif, N., Tyliszczak, T., Bourdelle, F., 2015. Characterization of Ca-phosphate biological materials by scanning transmission X-ray microscopy (STXM) at the Ca $L_{2,3}$-, P $L_{2,3}$- and C K-edges. Acta Biomater. 12, 260–269. https://doi.org/10.1016/j.actbio.2014.10.003.
D'Hondt, S., Inagaki, F., Zarikian, C.A., Abrams, L.J., Dubois, N., Engelhardt, T., Evans, H., Ferdelman, T., Gribsholt, B., Harris, R.N., Hoppie, Bryce W., Hyun, J.-H., Kallmeyer, J., Kim, J., Lynch, J.E., McKinley, Claire C., Mitsunobu, S., Morono, Y., Murray, R.W., Pockalny, R., Sauvage, J., Shimono, T., Shiraishi, F., Smith, D.C., Smith-Duque, Christopher E., Spivack, A.J., Steinsbu, B.O., Suzuki, Y., Szpak, M., Toffin, L., Uramoto, G., Yamaguchi, Y.T., Zhang, G.-l., Zhang, X.-H., Ziebis, W., 2015. Presence of oxygen and aerobic communities from sea floor to basement in deep-sea sediments. Nat. Geosci. 8, 299. https://doi.org/10.1038/ngeo2387.
De Yoreo, J.J., Gilbert, P.U., Sommerdijk, N.A., Penn, R.L., Whitelam, S., Joester, D., Zhang, H., Rimer, J.D., Navrotsky, A., Banfield, J.F., 2015. Crystallization by particle attachment in synthetic, biogenic, and geologic environments. Science 349https://doi.org/10.1126/science.aaa6760. aaa6760.
Dynes, J.J., Lawrence, J.R., Korber, D.R., Swerhone, G.D.W., Leppard, G.G., Hitchcock, A.P., 2006. Quantitative mapping of chlorhexidine in natural river biofilms. Sci. Total Environ. 369, 369–383. https://doi.org/10.1016/j.scitotenv.2006.04.033.
Dzade, N.Y., Roldan, A., Leeuw, N.H., 2013. Adsorption of methylamine on mackinawite (FES) surfaces: a density functional theory study. J. Chem. Phys. 139, 124708. https://doi.org/10.1063/1.4822040.
Estes, E.R., Andeer, P.F., Nordlund, D., Wankel, S.D., Hansel, C.M., 2017. Biogenic manganese oxides as reservoirs of organic carbon and proteins in terrestrial and marine environments. Geobiology 15, 158–172. https://doi.org/10.1111/gbi.12195.
Ferris, F.G., Fyfe, W.S., Beveridge, T.J., 1987. Bacteria as nucleation sites for authigenic minerals in a metal-contaminated lake sediment. Chem. Geol. 63, 225–232. https://doi.org/10.1016/0009-2541(87)90165-3.
Fitzsimmons, J.N., John, S.G., Marsay, C.M., Hoffman, C.L., Nicholas, S.L., Toner, B.M., German, C.R., Sherrell, R.M., 2017. Iron persistence in a distal hydrothermal plume supported by dissolved-particulate exchange. Nat. Geosci. 10, 195–203. https://doi.org/10.1038/ngeo2900.
Garrels, R.M., Perry, E., 1974. Cycling of carbon, sulfur, and oxygen through geologic time. In: Goldberg, E.D. (Ed.), The Sea. Wiley Intersci., New York, pp. 303–316.
Gorlas, A., Jacquemot, P., Guigner, J.-M., Gill, S., Forterre, P., Guyot, F., 2018. Greigite nanocrystals produced by hyperthermophilic archaea of *Thermococcales* order. PLoS One 13, e0201549. https://doi.org/10.1371/journal.pone.0201549.
Gregory, D., Mukherjee, I., Olson, S.L., Large, R.R., Danyushevsky, L.V., Stepanov, A.S., Avila, J.N., Cliff, J., Ireland, T.R., Raiswell, R., 2019. The formation mechanisms of sedimentary pyrite nodules determined by trace element and sulfur isotope microanalysis. Geochim. Cosmochim. Acta 259, 53–68. https://doi.org/10.1016/j.gca.2019.05.035.
Gregory, D.D., Large, R.R., Halpin, J.A., Baturina, E.L., Lyons, T.W., Wu, S., Danyushevsky, L., Sack, P.J., Chappaz, A., Maslennikov, V.V., Bull, S.W., 2015. Trace element content of sedimentary pyrite in black shales. Econ. Geol. 110, 1389–1410. https://doi.org/10.2113/econgeo.110.6.1389.
Hartnett, H.E., Keil, R.G., Hedges, J.I., Devol, A.H., 1998. Influence of oxygen exposure time on organic carbon preservation in continental margin sediments. Nature 391, 572–575. https://doi.org/10.1038/35351.
Hatton, B., Rickard, D., 2008. Nucleic acids bind to nanoparticulate iron(II) monosulphide in aqueous solutions. Orig. Life Evol. Biosph. 38, 257–270. https://doi.org/10.1007/s11084-008-9132-7.
Hedges, J.I., Baldock, J.A., Gélinas, Y., Lee, C., Peterson, M., Wakeham, S.G., 2001. Evidence for non-selective preservation of organic matter in sinking marine particles. Nature 409, 801. https://doi.org/10.1038/35057247.
Hedges, J.I., Keil, R.G., 1995. Sedimentary organic matter preservation: an assessment and speculative synthesis. Mar. Chem. 49, 81–115. https://doi.org/10.1016/0304-4203(95)00008-F.
Hitchcock, A.P., 2017. aXis2000 Is Written in Interactive Data Language (IDL). It is available free for non-commercial use from:. http://unicorn.macmaster.ca/axis2000.html.
Hitchcock, A.P., Dynes, J.J., Lawrence, J.R., Obst, M., Swerhone, G.D.W., Korber, D.R., Leppard, G.G., 2009. Soft X-ray spectromicroscopy of nickel sorption in a natural river biofilm. Geobiology 7, 432–453. https://doi.org/10.1111/j.1472-4669.2009.00211.x.
Hoffman, C.L., Nicholas, S.L., Ohnemus, D.C., Fitzsimmons, J.N., Sherrell, R.M., German, C.R., Heller, M.I., Lee, J.M., Lam, P.J., Toner, B.M., 2018. Near-field iron and carbon chemistry of non-buoyant hydrothermal plume particle, Southern East Pacific Rise 15°S. Mar. Chem. 201, 183–197. https://doi.org/10.1016/j.marchem.2018.01.011.
Jørgensen, B.B., 1982. Mineralization of organic matter in the sea bed—the role of sulphate reduction. Nature 296, 643–645. https://doi.org/10.1038/296643a0.
Jørgensen, B.B., Findlay, A.J., Pellerin, A., 2019. The biogeochemical sulfur cycle of marine sediments. Front. Microbiol. 10. https://doi.org/10.3389/fmicb.2019.00849.
Kaznatcheev, K.V., Karunakaran, C., Lanke, U.D., Urquhart, S.G., Obst, M., Hitchcock, A.P., 2007. Soft X-ray spectromicroscopy beamline at the CLS: commissioning results. Nucl. Instrum. Meth. A 582, 96–99. https://doi.org/10.1016/j.nima.2007.08.083.
Keil, R., 2017. Anthropogenic forcing of carbonate and organic carbon preservation in marine sediments. Annu. Rev. Mar. Sci. 9, 151–172. https://doi.org/10.1146/annurev-marine-010816-060724.
Keil, R., Mayer, L., 2014. Mineral matrices and organic matter. In: Falkowski, P.G., Freeman, K.H. (Eds.), Treatise on Geochemistry: Organic Geochemistry. Elsevier Science, pp. 337–359.
Keil, R.G., Montluçon, D.B., Prahl, F.G., Hedges, J.I., 1994. Sorptive preservation of labile organic matter in marine sediments. Nature 370, 549. https://doi.org/10.1038/370549a0.
Konhauser, K., Riding, R., 2012. Bacterial biomineralization. Fundamentals of Geobiology. John Wiley & Sons, Ltd, pp. 105–130.
Krepski, S.T., Emerson, D., Hredzak-Showalter, P.L., Luther, G.W., Chan III, C.S., 2013. Morphology of biogenic iron oxides records microbial physiology and environmental conditions: toward interpreting iron microfossils. Geobiology 11, 457–471. https://doi.org/10.1111/gbi.12043.
Lalonde, K., Mucci, A., Ouellet, A., Gelinas, Y., 2012. Preservation of organic matter in sediments promoted by iron. Nature 483, 198–200. https://doi.org/10.1038/Nature10855.
Large, R.R., Mukherjee, I., Gregory, D.D., Steadman, J.A., Maslennikov, V.V., Meffre, S., 2017. Ocean and atmosphere geochemical proxies derived from trace elements in marine pyrite: implications for ore genesis in sedimentary basins. Econ. Geol. 112, 423–450. https://doi.org/10.2113/econgeo.112.2.423.
Lawrence, J.R., Swerhone, G.D.W., Leppard, G.G., Araki, T., Zhang, X., West, M.M., Hitchcock, A.P., 2003. Scanning transmission X-ray, laser scanning, and transmission electron microscopy mapping of the exopolymeric matrix of microbial biofilms. Appl Environ Microb 69, 5543–5554. https://doi.org/10.1128/Aem.69.9.5543-5554.2003.
Lennie, A.R., Redfern, S.A.T., Champness, P.E., Stoddart, C.P., Schofield, P.F., Vaughan, D.J., 1997. Transformation of mackinawite to greigite: an in situ X-ray powder diffraction and transmission electron microscope study. Am. Mineral. 82, 302–309. https://doi.org/10.2138/am-1997-3-408.
Li, J., Benzerara, K., Bernard, S., Beyssac, O., 2013. The link between biomineralization and fossilization of bacteria: insights from field and experimental studies. Chem. Geol. 359, 49–69. https://doi.org/10.1016/j.chemgeo.2013.09.013.
Lomstein, B.A., Langerhuus, A.T., D'Hondt, S., Jorgensen, B.B., Spivack, A.J., 2012. Endospore abundance, microbial growth and necromass turnover in deep sub-sea-floor sediment. Nature 484, 101–104. https://doi.org/10.1038/Nature10905.
MacLean, L.C.W., Tyliszczak, T., Gilbert, P.U.P.A., Zhou, D., Pray, T.J., Onstott, T.C., Southam, G., 2008. A high-resolution chemical and structural study of framboidal pyrite formed within a low-temperature bacterial biofilm. Geobiology 6, 471–480. https://doi.org/10.1111/j.1472-4669.2008.00174.x.
Mansor, M., Berti, D., Hochella Jr, M.F., Murayama, M., Xu, J., 2019. Phase, morphology, elemental composition, and formation mechanisms of biogenic and abiogenic Fe-Cu-sulfide nanoparticles: a comparative study on their occurrences under anoxic conditions. Am. Mineral. 104, 703–717. https://doi.org/10.2138/am-2019-6848.
Mateo-Martí, E., Briones, C., Rogero, C., Gomez-Navarro, C., Methivier, C., Pradier, C.M., Martin-Gago, J.A., 2008. Nucleic acid interactions with pyrite surfaces. Chem. Phys. 352, 11–18. https://doi.org/10.1016/j.chemphys.2008.05.004.
Miot, J., Benzerara, K., Morin, G., Kappler, A., Bernard, S., Obst, M., Ferard, C., Skouri-Panet, F., Guigner, J.M., Posth, N., Galvez, M., Brown, G.E., Guyot, F., 2009. Iron biomineralization by anaerobic neutrophilic iron-oxidizing bacteria. Geochim. Cosmochim. Acta 73, 696–711. https://doi.org/10.1016/j.gca.2008.10.033.
Miot, J., Bernard, S., Bourreau, M., Guyot, F., Kish, A., 2017. Experimental maturation of Archaea encrusted by Fe-phosphates. Sci. Rep. 7, 16984. https://doi.org/10.1038/s41598-017-17111-9.
Miot, J., Maclellan, K., Benzerara, K., Boisset, N., 2011. Preservation of protein globules and peptidoglycan in the mineralized cell wall of nitrate-reducing, iron(II)-oxidizing bacteria: a cryo-electron microscopy study. Geobiology 9, 459–470. https://doi.org/10.1111/j.1472-4669.2011.00298.x.
Moreau, J.W., Webb, R.I., Banfield, J.F., 2004. Ultrastructure, aggregation-state, and crystal growth of biogenic nanocrystalline sphalerite and wurtzite. Am. Mineral. 89, 950–960. https://doi.org/10.2138/am-2004-0704.
Moreau, J.W., Weber, P.K., Martin, M.C., Gilbert, B., Hutcheon, I.D., Banfield, J.F., 2007. Extracellular proteins limit the dispersal of biogenic nanoparticles. Science 316, 1600–1603. https://doi.org/10.1126/science.1141064.
Mycke, B., Michaelis, W., Degens, E.T., 1988. Biomarkers in sedimentary sulfides of Precambrian age. Org. Geochem. 13, 619–625. https://doi.org/10.1016/0146-6380(88)90081-2.
Peiffer, S., Behrends, T., Hellige, K., Larese-Casanova, P., Wan, M., Pollok, K., 2015. Pyrite formation and mineral transformation pathways upon sulfidation of ferric hydroxides depend on mineral type and sulfide concentration. Chem. Geol. 400, 44–55. https://doi.org/10.1016/j.chemgeo.2015.01.023.
Picard, A., Gartman, A., Clarke, D.R., Girguis, P.R., 2018. Sulfate-reducing bacteria influence the nucleation and growth of mackinawite and greigite. Geochim. Cosmochim. Acta 220, 367–384. https://doi.org/10.1016/j.gca.2017.10.006.
Picard, A., Gartman, A., Girguis, P.R., 2016a. What do we really know about the role of microorganisms in iron sulfide mineral formation? Front. Earth Sci. 4, 68. https://doi.org/10.3389/feart.2016.00068.
Picard, A., Kappler, A., Schmid, G., Quaroni, L., Obst, M., 2015. Experimental diagenesis of organo-mineral structures formed by microaerophilic Fe(II)-oxidizing bacteria. Nat. Comm. 6, 6277. https://doi.org/10.1038/ncomms7277.
Picard, A., Obst, M., Schmid, G., Zeitvogel, F., Kappler, A., 2016b. Limited influence of Si on the preservation of Fe mineral-encrusted microbial cells during experimental diagenesis. Geobiology 14, 276–292. https://doi.org/10.1111/gbi.12171.

Pickering, I.J., George, G.N., Yu, E.Y., Brune, D.C., Tuschak, C., Overmann, J., Beatty, J.T., Prince, R.C., 2001. Analysis of sulfur biogeochemistry of sulfur bacteria using X-ray absorption spectroscopy. Biochemistry 40, 8138–8145. https://doi.org/10.1021/bi0105532.

Plekan, O., Feyer, V., Šutara, F., Skála, T., Švec, M., Cháb, V., Matolín, V., Prince, K.C., 2007. The adsorption of adenine on mineral surfaces: iron pyrite and silicon dioxide. Surf. Sci. 601, 1973–1980. https://doi.org/10.1016/j.susc.2007.02.032.

Ransom, B., Bennett, R., Baerwald, R., Shea, K., 1997. TEM study of in situ organic matter on continental margins: occurrence and the "monolayer" hypothesis. Mar. Geol. 138, 1–9. https://doi.org/10.1016/S0025-3227(97)00012-1.

Ransom, B., Bennett, R.H., Baerwald, R., Hulbert, M.H., Burkett, P.-J., 1999. In situ conditions and interactions between microbes and minerals in fine-grained marine sediments: a TEM microfabric perspective. Am. Mineral. 84, 183–192. https://doi.org/10.2138/am-1999-1-220.

Ravel, B., Newville, M., 2005. ATHENA, ARTEMIS, HEPHAESTUS: data analysis for X-ray absorption spectroscopy using IFEFFIT. J. Synchrotron Radiat. 12, 537–541. https://doi.org/10.1107/S0909049505012719.

Raven, M.R., Sessions, A.L., Fischer, W.W., Adkins, J.F., 2016. Sedimentary pyrite $\delta^{34}S$ differs from porewater sulfide in Santa Barbara Basin: Proposed role of organic sulfur. Geochim. Cosmochim. Acta 186, 120–134. https://doi.org/10.1016/j.gca.2016.04.037.

Rickard, D., Luther, G.W., 1997. Kinetics of pyrite formation by the H_2S oxidation of iron (II) monosulfide in aqueous solutions between 25 and 125°C: the mechanism. Geochim. Cosmochim. Acta 61, 135–147. https://doi.org/10.1016/S0016-7037(96)00322-5.

Rickard, D.T., 2012a. The geochemistry of sulfidic sedimentary rocks. In: Rickard, D.T. (Ed.), Developments in Sedimentology. Elsevier, Oxford, pp. 605–632.

Rickard, D.T., 2012b. Metastable sedimentary iron sulfides. In: Rickard, D.T. (Ed.), Developments in Sedimentology. Elsevier, Oxford, pp. 195–231.

Rickard, D.T., 2012c. Microbial sulfate reduction in sediments. In: Rickard, D.T. (Ed.), Developments in Sedimentology. Elsevier, Oxford, pp. 319–351.

Rickard, D.T., 2012d. Sedimentary pyrite. In: Rickard, D.T. (Ed.), Developments in Sedimentology. Elsevier, Oxford, pp. 233–285.

Riedinger, N., Brunner, B., Krastel, S., Arnold, G.L., Wehrmann, L.M., Formolo, M.J., Beck, A., Bates, S.M., Henkel, S., Kasten, S., 2017. Sulfur cycling in an iron oxide-dominated, dynamic marine depositional system: the Argentine continental margin. Front. Earth Sci. 5, 33. https://doi.org/10.3389/feart.2017.00033.

Rueden, C.T., Schindelin, J., Hiner, M.C., DeZonia, B.E., Walter, A.E., Arena, E.T., Eliceiri, K.W., 2017. ImageJ2: ImageJ for the next generation of scientific image data. BMC Bioinformatics 18, 529. https://doi.org/10.1186/s12859-017-1934-z.

Schoonen, M.A.A., 2004. Mechanisms of sedimentary pyrite formation. Geol. Soc. Am. Spec. Pap. 379, 117–134. https://doi.org/10.1130/0-8137-2379-5.117.

Shawar, L., Halevy, I., Said-Ahmad, W., Feinstein, S., Boyko, V., Kamyshny, A., Amrani, A., 2018. Dynamics of pyrite formation and organic matter sulfurization in organic-rich carbonate sediments. Geochim. Cosmochim. Acta 241, 219–239. https://doi.org/10.1016/j.gca.2018.08.048.

Sinninghe Damste, J.S., De Leeuw, J.W., 1990. Analysis, structure and geochemical significance of organically-bound sulphur in the geosphere: state of the art and future research. Org. Geochem. 16, 1077–1101. https://doi.org/10.1016/0146-6380(90)90145-P.

Stanley, W., Southam, G., 2018. The effect of gram-positive (*Desulfosporosinus orientis*) and gram-negative (*Desulfovibrio desulfuricans*) sulfate-reducing bacteria on iron sulfide mineral precipitation. Can. J. Microbiol. 64, 629–637. https://doi.org/10.1139/cjm-2017-0545.

Thiel, J., Byrne, J.M., Kappler, A., Schink, B., Pester, M., 2019. Pyrite formation from FeS and H_2S is mediated through microbial redox activity. Proc. Natl. Acad. Sci. U. S. A. 116, 6897–6902. https://doi.org/10.1073/pnas.1814412116.

Todd, E., Sherman, D., Purton, J., 2003. Surface oxidation of chalcopyrite ($CuFeS_2$) under ambient atmospheric and aqueous (pH 2-10) conditions: Cu, Fe L-and O K-edge X-ray spectroscopy. Geochim. Cosmochim. Acta 67, 2137–2146. https://doi.org/10.1016/S0016-7037(02)01371-6.

Toner, B.M., Fakra, S.C., Manganini, S.J., Santelli, C.M., Marcus, M.A., Moffett, J.W., Rouxel, O., German, C.R., Edwards, K.J., 2009. Preservation of iron(II) by carbon-rich matrices in a hydrothermal plume. Nat. Geosci. 2, 197–201. https://doi.org/10.1038/ngeo433.

Wächtershäuser, G., 1988. Pyrite formation, the first energy source for life: a hypothesis. Syst. Appl. Microbiol. 10, 207–210. https://doi.org/10.1016/S0723-2020(88)80001-8.

Wakeham, S.G., Canuel, E.A., 2006. Degradation and preservation of organic matter in marine sediments. In: Volkman, J.K. (Ed.), Marine Organic Matter: Biomarkers, Isotopes and DNA. Springer, Berlin, Heidelberg, pp. 295–321.

Wan, M., Schröder, C., Peiffer, S., 2017. Fe(III):S(-II) concentration ratio controls the pathway and the kinetics of pyrite formation during sulfidation of ferric hydroxides. Geochim. Cosmochim. Acta 217, 334–348. https://doi.org/10.1016/j.gca.2017.08.036.

Wehrmann, L.M., Riedinger, N., Brunner, B., Kamyshny Jr, A., Hubert, C.R., Herbert, L.C., Brüchert, V., Jørgensen, B.B., Ferdelman, T.G., Formolo, M.J., 2017. Iron-controlled oxidative sulfur cycling recorded in the distribution and isotopic composition of sulfur species in glacially influenced fjord sediments of west Svalbard. Chem. Geol. 466, 678–695. https://doi.org/10.1016/j.chemgeo.2017.06.013.

Werne, J.P., Hollander, D.J., Lyons, T.W., Damsté, J.S., 2004. Organic sulfur biogeochemistry: recent advances and future research directions. Geol. Soc. Am. Spec. Pap. 135–150. https://doi.org/10.1130/0-8137-2379-5.135.

Widdel, F., Bak, F., 1992. Gram-negative mesophilic sulfate-reducing bacteria. In: Balows, A., Trüper, H., Dworkin, M., Harder, W., Schleifer, K.-H. (Eds.), The Prokaryotes. Springer, New York, pp. 3352–3378.

Wolthers, M., Charlet, L., Van der Linde, P.R., Rickard, D., Van der Weijden, C.H., 2005. Surface chemistry of disordered mackinawite (FeS). Geochim. Cosmochim. Acta 69, 3469–3481. https://doi.org/10.1016/j.gca.2005.01.027.

Zeitvogel, F., Schmid, G., Hao, L., Ingino, P., Obst, M., 2016. ScatterJ: an ImageJ plugin for the evaluation of analytical microscopy datasets. J. Microsc. 261, 148–156. https://doi.org/10.1111/jmi.12187.

Zhou, J., Duchesne, P.N., Hu, Y., Wang, J., Zhang, P., Li, Y., Regier, T., Dai, H., 2014. Fe–N bonding in a carbon nanotube–graphene complex for oxygen reduction: an XAS study. Phys. Chem. Chem. Phys. 16, 15787–15791. https://doi.org/10.1039/C4CP01455C.

Zhu, X., Hitchcock, A.P., Le Nagard, L., Bazylinski, D.A., Morillo, V., Abreu, F., Leao, P., Lins, U., 2018. X-ray absorption spectroscopy and magnetism of synthetic greigite and greigite magnetosomes in magnetotactic bacteria. Geomicrobiol. J. 35, 215–226. https://doi.org/10.1080/01490451.2017.1362078.

Zopfi, J., Ferdelman, T., Fossing, H., 2004. Distribution and fate of sulfur intermediates - sulfite, tetrathionate, thiosulfate, and elemental sulfur - in marine sediments. Geol. Soc. Am. Spec. Pap. 379, 97–116. https://doi.org/10.1130/0-8137-2379-5.97.